SCIENTIFIC REPORTS

OPEN

Received: 27 February 2015
Accepted: 05 August 2015
Published: 08 September 2015

A unified data representation theory for network visualization, ordering and coarse-graining

István A. Kovács[1,2,3], Réka Mizsei[4] & Péter Csermely[5]

Representation of large data sets became a key question of many scientific disciplines in the last decade. Several approaches for network visualization, data ordering and coarse-graining accomplished this goal. However, there was no underlying theoretical framework linking these problems. Here we show an elegant, information theoretic data representation approach as a unified solution of network visualization, data ordering and coarse-graining. The optimal representation is the hardest to distinguish from the original data matrix, measured by the relative entropy. The representation of network nodes as probability distributions provides an efficient visualization method and, in one dimension, an ordering of network nodes and edges. Coarse-grained representations of the input network enable both efficient data compression and hierarchical visualization to achieve high quality representations of larger data sets. Our unified data representation theory will help the analysis of extensive data sets, by revealing the large-scale structure of complex networks in a comprehensible form.

Complex network[1,2] representations are widely used in physical, biological and social systems, and are usually given by huge data matrices. Network data size grew to the extent, which is too large for direct comprehension and requires carefully chosen representations. One option to gain insight into the structure of complex systems is to order the matrix elements to reveal the concealed patterns, such as degree-correlations[3,4] or community structure[5–11]. Currently, there is a diversity of matrix ordering schemes of different backgrounds, such as graph theoretic methods[12], sparse matrix techniques[13] and spectral decomposition algorithms[14]. Coarse-graining or renormalization of networks[15–20] also gained significant attention recently as an efficient tool to zoom out from the network, by averaging out short-scale details to reduce the size of the network to a tolerable extent and reveal the large-scale patterns. A variety of heuristic coarse-graining techniques – also known as multi-scale approaches – emerged, leading to significant advances of network-related optimization problems[21,22] and the understanding of network structure[19,20,23]. As we discuss in the Supplementary Information in more details, coarse-graining is also closely related to some block-models useful for clustering and benchmark graph generation[24–26].

The most essential tool of network comprehension is a faithful visualization of the network[27]. Preceding more elaborate quantitative studies, it is capable of yielding an intuitive, direct qualitative understanding of complex systems. Although being of a primary importance, there is no general theory for network layout, leading to a multitude of graph drawing techniques. Among these, force-directed[28] methods are probably the most popular visualization tools, which rely on physical metaphors. Graph layout aims to produce aesthetically appealing outputs, with many subjective aims to quantify, such as

[1]Wigner Research Centre, Institute for Solid State Physics and Optics, H-1525 Budapest, P.O.Box 49, Hungary. [2]Institute of Theoretical Physics, Szeged University, H-6720 Szeged, Hungary. [3]Center for Complex Networks Research and Department of Physics, Northeastern University, 177 Huntington Avenue, Boston, MA 02115, USA. [4]Institute of Organic Chemistry, Research Centre for Natural Sciences, Hungarian Academy of Sciences, Pusztaszeri út 59-67, H-1025 Budapest, Hungary. [5]Department of Medical Chemistry, Semmelweis University, H-1444 Budapest, P.O.Box 266, Hungary. Correspondence and requests for materials should be addressed to I.A.K. (email: kovacs.istvan@wigner.mta.hu)

minimal overlaps between not related parts (e.g. minimal edge crossings in $d = 2$), while preserving the symmetries of the network. Altogether, the field of graph drawing became a meeting point of art, physics and computer science[29].

Since the known approaches for the above problems generally lead to computationally expensive NP-hard problems[30], the practical implementations were necessarily restricted to advanced approximative heuristic algorithms. Moreover, there was no successful attempt to incorporate network visualization, data ordering and coarse-graining into a common theoretical framework. Since information theory provides ideal tools to quantify the hidden structure in probabilistic data[31,32], its application to complex networks[25,26,33–37] is a highly promising field. In this paper, our primary goal is to show an elegant, information theoretic representation theory for the unified solution of network visualization, data ordering and coarse-graining, establishing a common ground for the first time for these separated fields.

Usually, in graph theory, the complex system is at the level of abstraction, where each node is a dimensionless object, connected by lines representing their relations, given by the input data. Instead, we study the case in which both the input matrix and the approximative representation is given in the form of a probability distribution. This is the routinely considered case of edge weights reflecting the existence, frequency or strength of the interaction, such as in social and technological networks of communication, collaboration and traveling or in biological networks of interacting molecules or species. As discussed in details in the Supplementary Information, the probabilistic framework has long traditions in the theory of complex networks, including general random graph models, all Bayesian methods, community detection benchmarks[24], block-models[25,26] and graphons[38].

The major tenet of our unified framework is that the best representation is selected by the criteria, that it is the hardest to be distinguished from the input data. In information theory this is readily obtained by minimizing the relative entropy – also known as the Kullback-Leibler divergence[39] – as a quality function. In the following we show that the visualization, ordering and coarse-graining of networks are intimately related to each other, being organic parts of a straightforward, unified representation theory. We also show that in some special cases our unified framework becomes identical with some of the known state-of-the-art solutions for both visualization[40–42] and coarse-graining[25,26], obtained independently in the literature.

Results

General network representation theory. For simplicity, here we consider a symmetric adjacency matrix, A, having probabilistic entries $a_{ij} \geq 0$ and we try to find the optimal representation in terms of another matrix, B, having the same size. For more general inputs, such as hypergraphs given by an H incidence matrix, see the Methods section. The intuitive idea behind our framework is that we try to find the representation which is hardest to be distinguished from the input matrix. Within the frames of information theory, there is a natural way to quantify the closeness or *quality* of the representation, given by the relative entropy. The relative entropy, $D(A||B)$, measures the extra description length, when B is used to encode the data described by the original matrix, A, expressed by

$$D(A||B) = \sum_{ij} a_{ij} \ \ln \ \frac{a_{ij} b_{**}}{b_{ij} a_{**}} \geq 0, \tag{1}$$

where $a_{**} = \sum_{ij} a_{ij}$ and $b_{**} = \sum_{ij} b_{ij}$ ensure the proper normalizations of the probability distributions. As a shorthand notation here and in the following an asterisk indicates in index, for which the summation was carried out, as in the cases of $a_{i*} = \sum_j a_{ij}$ and $a_{*j} = \sum_i a_{ij}$. Although $D(A||B)$ is not a metric and not symmetric in A and B, it is an appropriate and widely applied measure of statistical remoteness[43], quantifying the distinguishability of B form A. The highest quality representation is achieved, when the relative entropy approaches 0, and our goal is to obtain a $B^\star$ representation satisfying

$$B^* = \mathrm{argmin}_B D(A||B). \tag{2}$$

Although $D(A||B) \geq 0$ can be in principle arbitrarily large, there is always a trivial upper bound available by the uncorrelated, *product state* representation, B^0, given by the matrix elements $b_{ij}^0 = \frac{1}{a_{**}} a_{i*} a_{*j}$. For an illustration see Fig. 1a. It follows simply from the definition of the $S(A)$, total information content and $I(A)$, mutual information, given in the Methods section, that $D_0 \equiv D(A||B^0) = I(A) \leq S(A)$. Consequently, the optimized value of $D(A||B^*) \leq D(A||B^0)$ can be always normalized with $I(A)$, or alternatively as

$$\eta \equiv D(A||B^*)/S(A) \leq 1. \tag{3}$$

Here η is the ratio of the needed extra description length to the optimal description length of the system. In the following applications we use η to compare the optimality of the found representations. As an important property, the optimization of relative entropy is local in the sense, that the global optimum of a network comprising independent subnetworks is also locally optimal for each subnetwork. The finiteness of D_0 also ensures, that if i and j are connected in the original network ($a_{ij} > 0$), then they are guaranteed

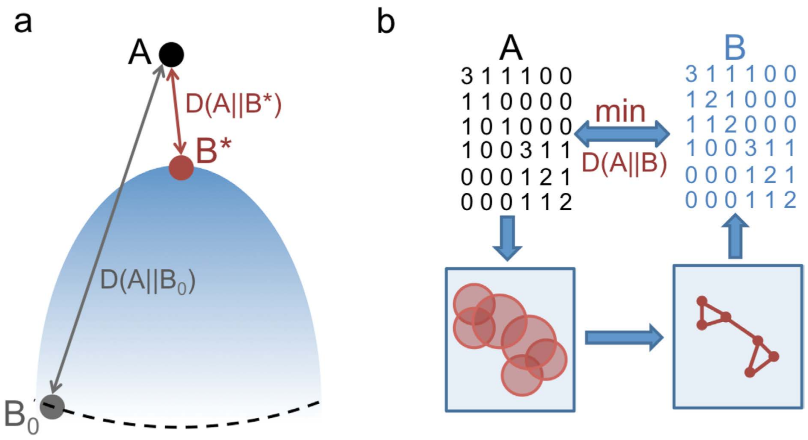

Figure 1. Illustration of our data representation framework. (**a**) For a given A input matrix, our goal is to find the closest B representation, measured by the $D(A||B)$ Kullback-Leibler divergence. The trivial representation, B_0, is always at a finite $D(A||B_0)$ value, limiting the search space. (**b**) In the data representation example of network visualization, we assign a distribution function to each network node, from which edge weights (B) are calculated based on the overlaps of the distributions. The best layout is given by the representation, which minimizes the $D(A||B)$ description length.

to be connected in a meaningful representation as well, enforcing $b_{ij} > 0$, otherwise D would diverge. In the opposite case, when we have a connection in the representation, without a corresponding edge in the original graph ($b_{ij} > 0$ while $a_{ij} = 0$), b_{ij} does not appear directly in D, only globally, as a part of the b_{**} normalization. This density-preserving property leads to a significant computational improvement for sparse networks, since there is no need to build a denser representation matrix, than the input matrix if we keep track of the b_{**} normalization. Nevertheless, the B matrix of the optimal representation (where D is small) is *close* to A, since due to Pinsker's inequality the total variation of the normalized distributions is bounded by D[44]

$$D(A||B) \geq \frac{a_{**}}{2\ln 2}\sum_{i,j}\left(\frac{a_{ij}}{a_{**}} - \frac{b_{ij}}{b_{**}}\right)^2. \tag{4}$$

Thus, in the optimal representation of a network all the connected network elements are connected, while having only a strongly suppressed amount of false positive connections. Here we note, that our representation theory can be straightforwardly extended for input networks given by an H incidence matrix instead of an adjacency matrix, for details of this case see the Methods section.

Network visualization and data ordering. Since force-directed layout schemes[28] have an energy or quality function, optimized by efficient techniques borrowed from many-body physics[45] and computer science[46], graph layout could be in principle serve as a quantitative tool. However some of, these popular approaches inherently struggle with an information shortage problem, since the edge weights only provide half the needed data to initialize these techniques. For instance, for the initialization of the widely applied Fruchterman-Reingold[47] (or for the Kamada-Kawai[48]) method we need to set both the strength of an attractive force (optimal distance) and a repulsive force (spring constant) between the nodes in order to have a balanced system. Due to the lack of sufficient information, such graph layout techniques become somewhat ill-defined and additional subjective considerations are needed to double the information encoded in the input data, traditionally by a nonlinear transformation of the attractive force parameters onto the parameters of the repulsive force[47]. Global optimization techniques, such as information theoretic methods[40–42,49] can, in principle, solve this problem by deriving the needed forces from one single information theoretic quality function.

In strong contrast to usual graph layout schemes, where the nodes are represented by points (without spatial extension) in a d-dimensional background space, connected by (straight, curved or more elaborated) lines, in our approach network nodes are extended objects, namely probability distributions ($\rho(x)$) over the background space. The d-dimensional background space is parametrized by the d-dimensional coordinate vector, x. Importantly, in our representation the shape of nodes encodes just that additional set of information, which has been lost and then arbitrarily re-introduced in the above mentioned force-directed visualization methods. In the following we consider the simple case of Gaussian distributions – having a width of σ, and norm $h = \int \mathrm{d}x^d \rho(x)$, see Eq. (6) of the Methods section –, but we have also tested the non-differentiable case of a homogeneous distribution in a spherical region of radius σ

leading to similar results. For a given graphical representation the b_{ij} edge weights are defined as the overlaps of the distributions ρ_i and ρ_j, given in the Methods section. For a schematic illustration see Fig. 1b.

The trivial data representation of B^0 can be obtained by an initialization, where all the nodes are at the same position, with the same distribution function (apart from a varying $h_i \propto a_{i*}$ normalization to ensure the proper statistical weight of the nodes). This way, initially $D_0 = I(A)$ is the mutual information of the input matrix, irrespectively from the chosen distribution function. The numerical optimization can be straightforwardly carried out by a fast and inefficient greedy optimization or a relatively slow, but more efficient simulated annealing scheme starting with an initialization of B^0. As a reasonable compromise, in the differentiable case of Gaussian distributions we use a Newton-Raphson iteration as in the Kamada-Kawai method[48] (for details see the Supplementary Information), having a run-time of $\mathcal{O}(N^2)$ for N nodes. Here we note, that similarly to the related t-SNE method[41,50], discussed in the Supplementary Information, the optimization can be in principle carried out in $\mathcal{O}(N \ \log \ N)$ time by applying the Barnes-Hut approximation[45].

Independently from the chosen optimization protocol, the finiteness of D_0 ensures that the connected nodes overlap in the layout as well, even for distributions having a finite support. Moreover, independent parts of the network (nodes or sets of nodes without connections between them) tend to be apart from each other in the layout. The density-preserving property of the representation leads to the fact, that even if all the nodes overlap with all other nodes in the layout, the B matrix can be kept exactly as sparse as the A matrix, while keeping track only of the sum of the b_{**} normalization including the rest of the potential b_{ij} matrix elements. Additionally, if two rows (and columns) of the input matrix are proportional to each other, then it is optimal to represent them with the same distribution function in the layout, as though the two rows were merged together.

In the differentiable case, e.g. with Gaussian distributions, our visualization method can be conveniently interpreted as a force-directed method. If the normalized overlap, b_{ij}/b_{**}, is smaller at a given edge than the normalized edge weight, a_{ij}/a_{**}, then it leads to an attractive force, while the opposite case induces a repulsive force. For details see the Supplementary Information. For Gaussian distributions all nodes overlap in the representations, leading typically to $D > 0$ in the optimal representation. However, for distributions with a finite support, such as the above mentioned homogeneous spheres, perfect layouts with $D = 0$ can be easily achieved even for sparse graphs. In $d = 2$ dimensions this concept is reminiscent to the celebrated concept of planarity[51]. However, our concept can be applied in any dimensions. Furthermore, it goes much beyond planarity, since any network of $D_0 \equiv I(A) = 0$ (e.g. a fully connected graph) is perfectly represented in any dimensions by B^0, that is by simply putting all the nodes at the same position.

Our method is illustrated in Fig. 2. on the Zachary karate club network[52], which became a cornerstone of graph algorithm testing. It is a weighted social network of friendships between $N_0 = 34$ members of a karate club at a US university, which fell apart after a debate into two communities. While usually the size of the nodes can be chosen arbitrarily, e.g. to illustrate their degree or other relevant characteristics, here the size of the nodes is part of the visualization optimization by reflecting the width of the distribution, indicating relevant information about the layout itself. In fact, the size of a node represents the uncertainty of its position, serving also as a readily available local quality indicator. For illustration of the applicability of our network visualization method to larger collaboration[53] and information sharing[54] networks, having more than 10,000 nodes, see the Supplementary Information.

Our network layout technique works in any dimensions, as illustrated in $d = 1$, 2 and 3 in Fig. 2. In each case the communities are clearly recovered and, as expected, the quality of layout becomes better (indicated by a decreasing η value) as the dimensionality of the embedding space increases. Nevertheless, the one dimensional case deserves special attention, since it serves as an ordering of the elements as well (after resolving possible degenerations with small perturbations), as illustrated in Fig. 1e.

Since $D(A||B) = H(A, B) - S(A)$, $H(A, B)$ is the (unnormalized) cross-entropy, we can equivalently minimize the cross-entropy for B. For a comparison to the known cross-entropy methods[55–57] see the Supplementary Information. However, as a consequence, the visualization and ordering is perfectly robust against noise in the input matrix elements. This means, that even if the input A matrix is just the average of a matrix ensemble, where the a_{ij} elements have an (arbitrarily) broad distribution, the optimal representation is the same as it were by optimizing for the whole ensemble simultaneously. This extreme robustness follows straightforwardly from the linearity of the $H(A, B)$ cross-entropy in the a_{ij} matrix elements. Note, however, that the optimal value of the $D(A||B^*)$ distinguishability is generally shifted by the noise.

When applying a local scheme for the optimization of the representations, we generally run into local minima, in which the layout can not be improved by single node updates, since whole parts of the network should be updated (rescaled, rotated or moved over each other), instead. Being a general difficulty in many optimization problems, it was expected to be insurmountable also in our approach. In the following we show, that the relative entropy based coarse-graining scheme – given in the next section – can, in practice, efficiently help us trough these difficulties in polynomial time.

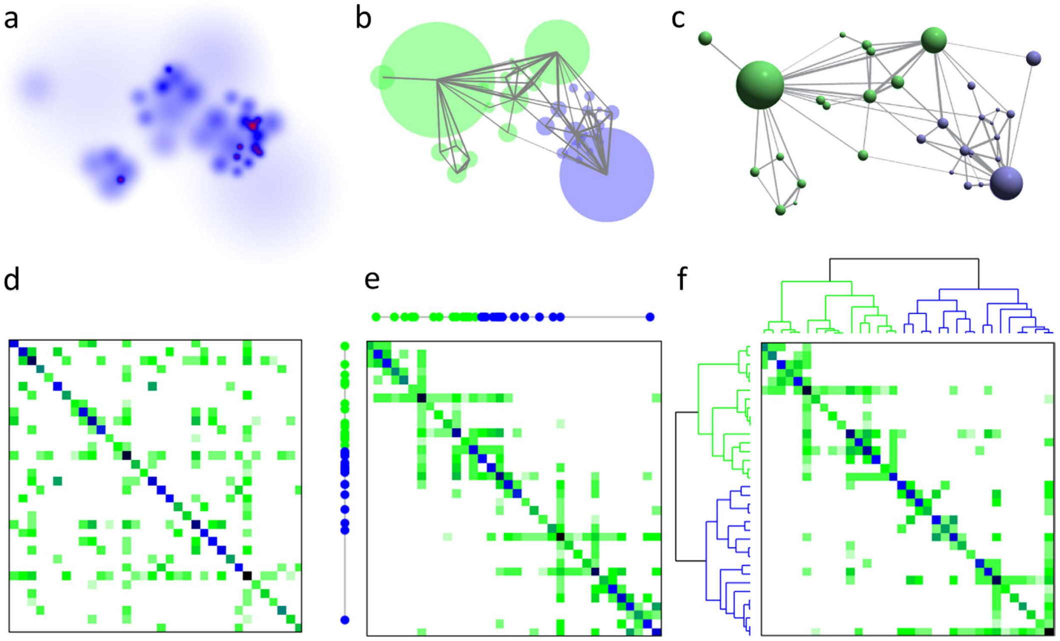

Figure 2. Illustration of the power of our unified representation theory on the Zachary karate club network[52]. The optimal layout ($\eta = 2.1\%$, see Eq. (3)) in terms of $d = 2$ dimensional Gaussians is shown by a density plot in (**a**) and by circles of radiuses σ_i in (**b**). (**c**) the best layout is obtained in $d = 3$ ($\eta = 1.7\%$), where the radiuses of the spheres are chosen to be proportional to σ_i. (**d**) the original data matrix of the network with an arbitrary ordering. (**e**) the $d = 1$ layout ($\eta = 4.5\%$) yields an ordering of the original data matrix of the network. (**f**) the optimal coarse-gaining of the data matrix yields a tool to zoom out from the network in accordance with the underlying community structure. The colors indicate our results at the level of two clusters, being equivalent to the ones given by popular community detection techniques, such as the modularity optimization[5] or the degree-corrected stochastic block model[25]. We note, that the coarse-graining itself does not yield a unique ordering of the nodes, therefore an arbitrarily chosen compatible ordering is shown in this panel.

Coarse-graining of networks. In the process of coarse-graining we identify groups or clusters of nodes, and try to find the best representation, while averaging out for the details inside the groups. Inside a group, the nodes are replaced by their normalized average, while keeping their degrees fixed. As the simplest example, the coarse-graining of two rows means, that instead of the original k and l rows, we use two new rows, being proportional to each other, while the $b_{k*} = a_{k*}$ and $b_{l*} = a_{l*}$ probabilities are kept fixed

$$b_{ki} = a_{k_*}\frac{a_{ki} + a_{li}}{a_{k_*} + a_{l_*}},\ b_{li} = a_{l_*}\frac{a_{ki} + a_{li}}{a_{k_*} + a_{l_*}}. \tag{5}$$

In other words, we first simply sum up the corresponding rows and obtain a smaller matrix, then inflate this fused matrix back to the original size while keeping the statistical weights of the nodes (degrees) fixed. For an illustration of the smaller, fused data matrices see the lower panels of Fig. 3a–d. For a symmetric adjacency matrix, the coarse-graining step can be also carried out simultaneously and identically for the rows and columns, known as a bi-clustering. The optimal bi-clustering is illustrated in Fig. 2f for the Zachary karate club network. The heights in the shown dendrogram indicate the D values of the representations when the fusion step happens.

For the general, technical formulation of our coarse-graining approach and details of the numerical optimization, see the Supplementary Information. As it turns out, for coarse-graining, $D(A||B)$ is nothing but the amount of lost mutual information between the rows and columns of the input matrix. In other words, $D(A||B)$ is the amount of lost structural signal during coarse-graining and finally we arrive at a complete loss of structural information, $D(A||B) = D_0$. Prevailingly, this final state coincides with the above proposed initialization step of our network layout approach. As a further connection with the graph layout, if two rows (or columns) are proportional to each other, they can be fused together without losing any information, since their coarse-graining leads to no change in the Kullback-Leibler divergence, D.

Since it is generally expected to be an NP-hard problem to find the optimal simplified, coarse-grained description of a network at a given scale, we have to rely on approximate heuristics having a reasonable

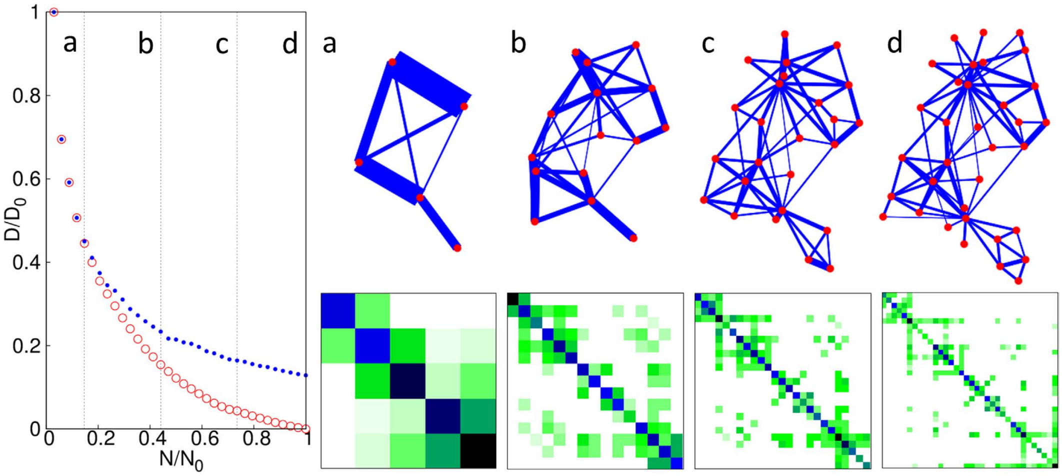

Figure 3. Illustration of our hierarchical visualization technique on the Zachary karate club network[52]. In our hierarchical visualization technique the coarse-graining procedure guides the optimization for the layout in a top-down way. As the N number of nodes increases, the relative entropy of both the coarse-grained description (red, ○) and the layout (blue, ●) decreases. The panels (**a–d**) show snapshots of the optimal layout and the corresponding coarse-grained input matrix at the level of $N = 5$, 15, 25 and 34 nodes, respectively. For simplicity, here the h_i normalization of each distribution is kept fixed to be $\propto a_{i*}$ during the process, leading finally to $\eta = 4.4\%$.

run-time. In the following we use a local coarse-graining approach, where in each step a pair of rows (and columns) is replaced by coarse-grained ones, giving the best approximative new network in terms of the obtained pairwise D-value. This way the optimization can be generally carried out in $\mathcal{O}(N^3)$ time for N nodes. As a common practice, for larger networks we could use the approximation of fusing together a finite amount (eg. 1%) of the nodes in each step instead of a single pair, leading to an improved $\mathcal{O}(N^2 \log N)$ run-time.

As illustrated in Fig. 2f the coarse-graining process creates a hierarchical dendrogram in a bottom-up way, representing the structure of the network at all scales. Here we note, that a direct optimization is also possible for our quality function at a fixed number of groups, creating a clustering. As described in the Supplementary Information in details, our coarse-graining scheme comprises also the case of the overlapping clustering, since it is straightforward to assign a given node to multiple groups as well. As noted there, when considering non-overlapping partitionings with a given number of clusters, our method gives back the degree-corrected stochastic block-model of Karrer and Newman[25] due to the degree-preservation. Consequently, our coarse-graining approach can be viewed as an overlapping and hierarchical reformulation and generalization of this successful state-of-the-art technique.

Hierarchical layout. Although the introduced coarse-graining scheme may be of significant interest whenever probabilistic matrices appear, here we focus on its application for network layout, to obtain a hierarchical visualization[58–63]. Our bottom-up coarse-graining results can be readily incorporated into the network layout scheme in a top-down way by initially starting with one node (comprising the whole system), and successively undoing the fusion steps until the original system is recovered. Between each such extension step the layout can be optimized as usual.

We have found, that this hierarchical layout scheme produces significantly improved layouts – in terms of the final D value – compared to a local optimization, such as a simple simulated annealing or Newton-Raphson iteration. By incorporating the coarse-graining in a top-down approach, we first arrange the position of the large-scale parts of the network, and refine the picture in later steps only. The refinement steps happen, when the position and extension of the large-scale parts have already been sufficiently optimized. After such a refinement step, the nodes – moved together so far – are treated separately. At a given scale (having $N \leq N_0$ nodes), the D value of the coarse-graining provides a lower bound for the D value of the obtainable layout. Our hierarchical visualization approach is illustrated in Fig. 3. with snapshots of the layout and the coarse-grained representation matrices of the Zachary karate club network[52] at $N = 5$, 15, 25 and 34. As an illustration on a larger and more challenging network, in Fig. 4. we show the result of the hierarchical visualization on the giant component of the weighted human diseasome network[64]. In this network we have $N_0 = 516$ nodes, representing diseases, connected by mutually associated genes. The colors indicate the known disease groups, which are found to be well colocalized in the visualization.

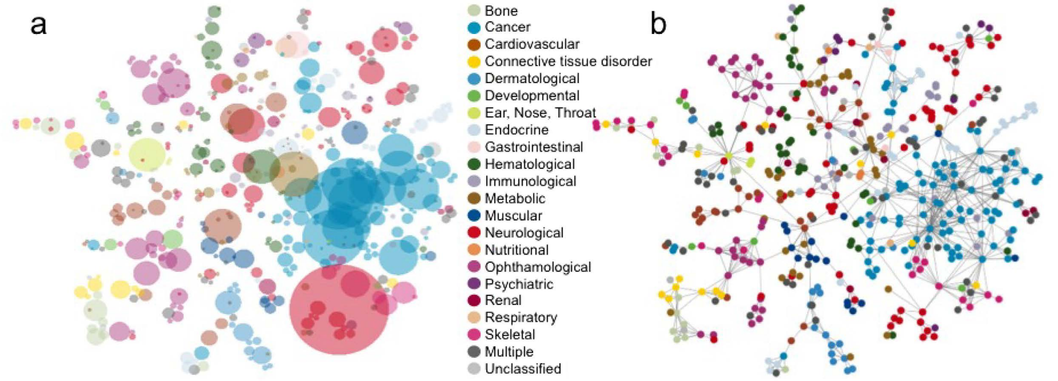

Figure 4. Visualization of the human diseasome. The best obtained layout ($\eta = 3.1\%$) by our hierarchical visualization technique of the human diseasome is shown by circles of radiuses σ_i in (**a**) and by a traditional graph in (**b**). The nodes represent diseases, colored according to known disease categories[64], while the σ_i width of the distributions in (**a**) indicates the uncertainty of the positions. In the numerical optimization for this network we primarily focused on the positioning of the nodes, thus the optimization for the widths and normalizations was only turned on as a fine-tuning after an initial layout was obtained.

Discussion

In this paper, we have introduced a unified, information theoretic solution for the long-standing problems of matrix ordering, network visualization and data coarse-graining. While establishing a connection between these separated fields for the first time, our unified framework also incorporates some of the known state-of-the art efficient techniques as special cases. In our framework, the steps of the applied algorithms were derived in an *ab inito* way from the same first principles, in strong contrast to the large variety of existing algorithms, lacking such an underlying theory, providing also a clear interpretation of the obtained results.

After establishing the general representation theory, in our paper we first demonstrated that the minimization of relative information yields a novel visualization technique, while representing the A input matrix by the B co-occurrence matrix of extended distributions, embedded in a d-dimensional space. As another application of the same approach, we obtained a hierarchical coarse-graining scheme, when the input matrix is represented by its subsequently coarse-grained versions. Since these applications are two sides of the same representation theory, they turned out to be superbly compatible, leading to an even more powerful hierarchical visualization technique, illustrated on the real-world example of the human diseasome network. Although we have focused on the visualization in d-dimensional flat, continuous space, the representation theory can be applied more generally, incorporating also the case of curved or discrete embedding spaces. As a possible future application, we mention the optimal embedding of a (sub)graph into another graph.

We have also shown that our relative entropy-based visualization with e.g. Gaussian node distributions can be naturally interpreted as a force-directed method. Traditional force directed methods prompted huge efforts on the computational side to achieve scalable algorithms applicable for the large data sets in real life. Here we can not and do not wish to compete with such advanced techniques, but we believe that our approach can be a good starting point for further scalable implementations. As a first step towards this goal, we have outlined the possible future directions of computational improvement. Moreover, in the Supplementary Information we illustrated the applicability of our approach on larger scale networks as well. We have also demonstrated, that network visualization is already interesting in one dimension yielding an ordering for the elements of the network. Our efficient coarse-graining scheme can also serve as an unbiased, resolution-limit-free, starting point for the infamously challenging problem of community detection by selecting the best cut of the dendrogram based on appropriately chosen criteria.

Our data representation framework has a broad applicability, starting form either the node-node or edge-edge adjacency matrices or the edge-node incidence matrix of weighted networks, incorporating also the cases of bipartite graphs and hypergraphs. We believe, that our unified representation theory is a powerful tool to gain a deeper understanding of the huge data matrices in science, beyond the limits of existing heuristic algorithms. Since in this paper our primary intention was merely to demonstrate a proof of concept study of our theoretical framework, more detailed analyses of interesting complex networks will be the subject of forthcoming articles.

Methods

We use the most general form of the input matrices, without assuming their normalization. In accordance, there is no need to normalize the information theoretic measures over $\mathcal{A}$, such as the $S(A) \equiv -\sum_{ij} a_{ij} \ln\left(a_{ij}/a_{**}\right)$ information content or the mutual information between the rows and columns of A given by $I(A) = \sum_{ij} a_{ij} \ln \frac{a_{ij}a_{**}}{a_{i_*}a_{*j}}$, where $a_{i_*} = \sum_j a_{ij}$ and $a_{*j} = \sum_i a_{ij}$. If we start with the H edge-node co-occurrence (incidence) matrix instead, suited to describe hypergraphs as well, then $A \sim H^T H$ is simply given by the elements, $a_{ij} = \frac{1}{h_{**}} \sum_k h_{ki} h_{kj}$, where $h_{**} = \sum_{ij} h_{ij}$. This way we generally have non-zero diagonal entries (a_{ii}). See the Supplementary Information for a discussion on the case with strictly zero diagonals.

The parametrization of the Gaussian distributions used in the visualization is the following in d-dimensions

$$\rho(\{x_i^0\}, \sigma, n) = \frac{n}{\sqrt{(2\pi)^d}} \exp\left(-\frac{\sum_{i=1}^{d}(x_i - x_i^0)^2}{2\sigma^2}\right). \tag{6}$$

For a given graphical representation the B co-occurrence matrix is built up from the overlaps of the distributions ρ_i and ρ_j – analogously to the construction of A from H – as $b_{ij} = \frac{1}{R}\int \mathrm{d}x^d \rho_i(x)\rho_j(x)$, where $R = \sum_k \int \mathrm{d}x^d \rho_k(x)$ is an (irrelevant) global normalization factor. Although our network layout works only for symmetric adjacency matrices, the ordering can be extended for hypergraphs with asymmetric H matrices as well, since the orderings of the two adjacency matrices HH^T and $H^T H$ readily yield orderings for both the rows and columns of the matrix, H.

For details of the numerical optimization for visualization and coarse-graining see the Supplementary Information. The codes written in C++ using OpenGL are freely available - as command-line programs - upon request.

References

1. Newman, M. E. J. *Networks: An Introduction*. (Oxford Univ. Press, 2010).
2. Albert, R. & Barabási, A.-L. Statistical mechanics of complex networks. *Reviews of Modern Physics* **74,** 47–97 (2002).
3. Newman, M. E. J. Assortative mixing in networks. *Phys. Rev. Lett.* **89,** 208701 (2002).
4. Reshef, D. N. *et al.* Detecting novel associations in large data sets. *Science* **334,** 1518–1524 (2011).
5. Girvan, M. & Newman, M. E. J. Community structure in social and biological networks. *Proc. Natl Acad. Sci. USA* **99,** 7821–7826 (2002).
6. Newman, M. E. J. Communities, modules and large-scale structure in networks. *Nature Physics* **8,** 25–31 (2012).
7. Fortunato, S. Community detection in graphs. *Phys. Rep.* **486,** 75–174 (2010).
8. Kovács, I. A., Palotai, R., Szalay, M. S. & Csermely, P. Community landscapes: an integrative approach to determine overlapping network module hierarchy, identify key nodes and predict network dynamics. *PLoS ONE* **5,** e12528 (2010).
9. Olhede, S. C. & Wolfe, P. J. Network histograms and universality of blockmodel approximation. *Proc. Natl Acad. Sci. USA* **111,** 14722–14727 (2014).
10. Bickel P. J., Chen A. A nonparametric view of network models and Newman-Girvan and other modularities. *Proc. Natl. Acad. Sci. USA* **106** (50), 21068–21073 (2009).
11. Bickel P. J. & Sarkar P. Hypothesis testing for automated community detection in networks. arXiv: 1311.2694. (2013) (Date of access: 15/02/2015).
12. King, I. P. An automatic reordering scheme for simultaneous equations derived from network analysis. *Int. J. Numer. Methods* **2,** 523–533 (1970).
13. George A. & Liu, J. W.-H. *Computer solution of large sparse positive definite systems*. (Prentice-Hall Inc, 1981).
14. West, D. B. *Introduction to graph theory* 2nd edn. (Prentice-Hall Inc, 2001).
15. Song, C., Havlin, S. & Makse, H. A. Self-similarity of complex networks. *Nature* **433,** 392–395 (2005).
16. Gfeller, D. & De Los Rios, P. Spectral coarse graining of complex networks. *Phys. Rev. Lett.* **99,** 038701 (2007).
17. Sales-Pardo, M., Guimera, R., Moreira, A. A. & Amaral L. A. N. Extracting the hierarchical organization of complex systems. *Proc. Natl. Acad. Sci. USA* **104,** 15224–15229 (2007).
18. Ravasz, E., Somera, A. L., Mongru, D. A., Oltvai, Z. N. & Barabási, A.-L. Hierarchical organization of modularity in metabolic networks. *Science* **297,** 1551–1555 (2002).
19. Radicchi, F., Ramasco, J. J., Barrat, A. & Fortunato, S. Complex networks renormalization: flows and fixed points. *Phys. Rev. Lett.* **101,** 148701 (2008).
20. Rozenfeld, H. D., Song, C. & Makse, H. A. Small-world to fractal transition in complex networks: a renormalization group approach. *Phys. Rev. Lett.* **104,** 025701 (2010).
21. Walshaw, C. A multilevel approach to the travelling salesman problem. *Oper. Res.* **50,** 862–877 (2002).
22. Walshaw, C. Multilevel refinement for combinatorial optimisation problems. *Annals of Operations Research* **131,** 325–372 (2004).
23. Ahn, Y.-Y., Bagrow J. P. & Lehmann S. Link communities reveal multiscale complexity in networks *Nature* **1038,** 1–5 (2010).
24. Lancichinetti, A., Fortunate, S. & Radicchi, F. Benchmark graphs for testing community detection algorithms, *Phys. Rev. E* **78,** 046110 (2008).
25. Karrer, B. & Newman, M. E. J. Stochastic blockmodels and community structure in networks. *Phys. Rev. E* **83,** 016107 (2011).
26. Larremore, D. B., Clauset, A. & Jacobs, A. Z. Efficiently inferring community structure in bipartite networks. *Phys. Rev. E* **90,** 012805 (2014).
27. Di Battista, G., Eades, P., Tamassia, R. & Tollis, I. G. *Graph Drawing: Algorithms for the Visualization of Graphs*. (Prentice-Hall Inc, 1998).
28. Kobourov, S. G. Spring embedders and force-directed graph drawing algorithms. arXiv: 1201.3011 (2012) (Date of access: 15/02/2015).
29. *Graph Drawing, Symposium on Graph Drawing GD'96* (ed North, S.), (Springer-Verlag, Berlin, 1997).
30. Garey, M. R. & Johnson, D. S. *Computers and Intractability: A Guide to the Theory of NP-Completeness*. (W.H. Freeman and Co., 1979).

31. Kinney, J. B. & Atwal, G. S. Equitability, mutual information, and the maximal information coefficient. *Proc. Natl. Acad. Sci. USA* **111,** 3354–3359 (2014).
32. Lee, D. D. & Seung, H. S. Learning the parts of objects by non-negative matrix factorization. *Nature* **401,** 788–791 (1999).
33. Slonim, N., Atwal, G. S., Tkačik, G. & Bialek, W. Information-based clustering. *Proc. Natl. Acad. Sci. USA* **102,** 18297–18302 (2005).
34. Rosvall, M. & Bergstrom, C. T. An information-theoretic framework for resolving community structure in complex networks. *Proc. Natl. Acad. Sci. USA* **104,** 7327–7331 (2007).
35. Rosvall, M., Axelsson, D. & Bergstrom, C. T. The map equation. *Eur. Phys. J. Special Topics* **178,** 13–23 (2009).
36. Zanin, M., Sousa, P. A. & Menasalvas, E. Information content: assessing meso-scale structures in complex networks. *Europhys. Lett.* **106,** 30001 (2014).
37. Allen, B., Stacey, B. C. & Bar-Yam, Y. An information-theoretic formalism for multiscale structure in complex systems. arXiv: 1409.4708 (2014) (Date of access: 15/02/2015).
38. Lovász, L. *Large networks and graph limits, volume 60 of American Mathematical Society Colloquium Publications*. American Mathematical Society, Providence, RI, (2012).
39. Kullback, S. & Leibler, R. A. On information and sufficiency. *Annals of Mathematical Statistics* **22,** 79–86 (1951).
40. Hinton, G. & Roweis, S. *Stochastic Neighbor Embedding, in Advances in Neural Information Processing Systems*, Vol. 15, *833-840* (The MIT Press, Cambridge, 2002).
41. van der Maaten, L. & Hinton, G. Visualizing Data using t-SNE, *Journal of Machine Learning Research* **9,** 2579–2605 (2008).
42. Yamada, T., Saito, K. & Ueda, N. Cross-entropy directed embedding of network data, *Proceedings of the 20th International Conference on Machine Learning (ICML2003)*, 832–839 (2003).
43. Grünwald, P. D. *The Minimum Description Length Principle*, (MIT Press, 2007).
44. Cover, Th. M. & Thomas, J. A. *Elements of Information Theory* 1st edn, Lemma 12.6.1, 300–301 (John Wiley & Sons, 1991).
45. Barnes, J. & Hut, P. A hierarchical O(NlogN) force-calculation algorithm. *Nature* **324,** 446–449 (1986).
46. Gansner, E. R., Koren, Y. & North, S. in *Graph drawing by stress majorization*, Vol. 3383 (ed Pach, J.), 239–250 (Springer-Verlag, 2004).
47. Fruchterman, T. M. & Reingold, E. M. Graph Drawing by Force-Directed Placement, *Software: Practice & Experience* **21,** 1129–1164 (1991).
48. Kamada, T. & Kawai, S. An algorithm for drawing general undirected graphs. *Information Processing Letters* (Elsevier) 31, 7–15 (1989).
49. Estévez, P. A., Figueroa, C. J. & Saito, K. Cross-entropy embedding of high-dimensional data using the neural gas model. *Neural Networks* **18,** 727–737 (2005).
50. van der Maaten, L. J. P. Accelerating t-SNE using Tree-Based Algorithms. *Journal of Machine Learning Research* **15,** 3221–3245 (2014).
51. Hopcroft, J. & Tarjan, R. E. Efficient planarity testing. *Journal of the Association for Computing Machinery* **21,** 549–568 (1974).
52. Zachary, W. W. An information flow model for conflict and fission in small groups. *Journal of Anthropological Research* **33,** 452–473 (1977).
53. Leskovec, J., Kleinberg, J. & Faloutsos, C. *Graph Evolution: Densification and Shrinking Diameters.* ACM Transactions on Knowledge Discovery from Data (ACM TKDD), 1(1), (2007). Data is available at: http://snap.stanford.edu/data/ca-HepPh.html.
54. Boguña, M., Pastor-Satorras, R., Diaz-Guilera, A. & Arenas, A. Models of social networks based on social distance attachment. *Phys. Rev. E* **70,** 056122 (2004). Data is available at: http://deim.urv.cat/alexandre.arenas/data/welcome.htm.
55. Kullback, S. *Information Theory and Statistics*, (John Wiley: New York, NY, USA, 1959).
56. Kapur, J. N. & Kesavan, H. K. The inverse MaxEnt and MinxEnt principles and their applications, in *Maximum Entropy and Bayesian Methods, Fundamental Theories in Physics*, Springer Netherlands, 39, 433–450 (1990).
57. Rubinstein, R. Y. The cross-entropy method for combinatorial and continuous optimization. *Method. Comput. Appl. Probab.* **1,** 127–190 (1999).
58. Gajer, P., Goodrich, M. T. & Kobourov, S. G. A multi-dimensional approach to force-directed layouts of large graphs, *Computational Geometry: Theory and Applications* **29**, 3–18 (2004).
59. Harel, D. & Koren, Y. A fast multi-scale method for drawing large graphs. *J. Graph Algorithms and Applications* **6,** 179–202 (2002).
60. Walshaw, C. A multilevel algorithm for force-directed graph drawing. *J. Graph Algorithms Appl.* **7,** 253–285 (2003).
61. Hu, Y. F. Efficient and high quality force-directed graph drawing. *The Mathematica Journal* **10,** 37–71 (2006).
62. Szalay-Bekö, M., Palotai, R., Szappanos, B., Kovács, I. A., Papp, B. & Csermely P., ModuLand plug-in for Cytoscape: determination of hierarchical layers of overlapping network modules and community centrality. *Bioinformatics* **28,** 2202–2204 (2012).
63. Six, J. M. & Tollis, I. G. in *Software Visualization*, Vol. 734, (ed Zhang, K.) Ch. 14, 413–437 (Springer US, 2003).
64. Goh, K.-I. *et al.* The human disease network. *Proc. Natl. Acad. Sci. USA* **104,** 8685–8690 (2007).

Acknowledgements

We are grateful to the members of the LINK-group (www.linkgroup.hu) and E. Güney for useful discussions. This work was supported by the Hungarian National Research Fund under grant Nos. OTKA K109577, K115378 and K83314. The research of IAK was supported by the European Union and the State of Hungary, co-financed by the European Social Fund in the framework of TÁMOP 4.2.4. A/2-11-1-2012-0001 'National Excellence Program'.

Author Contributions

I.A.K. and R.M. conceived the research and ran the numerical simulations. I.A.K. devised and implemented the applied algorithms. I.A.K. and P.Cs. wrote the main manuscript text. All authors reviewed the manuscript.

Additional Information

Supplementary information accompanies this paper at http://www.nature.com/srep

Competing financial interests: The authors declare no competing financial interests.

How to cite this article: Kovács, I. A. *et al.* A unified data representation theory for network visualization, ordering and coarse-graining. *Sci. Rep.* **5**, 13786; doi: 10.1038/srep13786 (2015).

Supplementary Information: A unified data representation theory for network visualization, ordering and coarse-graining

István A. Kovács*,[1, 2, 3] Réka Mizsei,[4] and Péter Csermely[5]

[1] *Wigner Research Centre, Institute for Solid State Physics and Optics, H-1525 Budapest, P.O.Box 49, Hungary*
[2] *Institute of Theoretical Physics, Szeged University, H-6720 Szeged, Hungary*
[3] *Center for Complex Networks Research and Department of Physics, Northeastern University,*
110 Forsyth Street, 111 Dana Research Center, Boston, MA 02115, USA
[4] *Institute of Organic Chemistry, Research Centre for Natural Sciences,*
Hungarian Academy of Sciences, Pusztaszeri út 59-67, H-1025 Budapest, Hungary
[5] *Department of Medical Chemistry, Semmelweis University, H-1444 Budapest, P.O.Box 266, Hungary*

(Dated: August 20, 2015)

PACS numbers: 89.75.Fb:Structures and organization in complex systems, 89.75.Hc:Networks and genealogical trees, 89.20.-a:Interdisciplinary applications of physics

Contents

* Electronic address: kovacs.istvan@wigner.mta.hu

I. OVERVIEW OF THE RELATED METHODS

A. Probabilistic approaches

Whenever we apply some random graphs, including benchmarks for clustering, or other generative network models, there is always an underlying probabilistic framework, from which the particular instances are drawn. The common element in these representations is the non-negativity of the matrix elements of the input matrix.

However, when applying information theory on the structure of complex networks, there are different ways of establishing it based on the identification of probability distribution(s) in the given input data, A. In the following we give a brief overview about the possibilities and discuss the existing methods for both visualization and coarse-graining. The possible definitions for the underlying probability distributions are the following.

- Network-level: The full matrix is one probability distribution, thus one system, which can be normalized by $a_{**} = \sum_{ij} a_{ij}$.
- Node-level: Each node, namely each row (or column), in the matrix is a separate probability distribution, which can be normalized independently by $a_{i*} = \sum_j a_{ij}$, $\forall i$. In this case each node is treated independently from the rest of the network.
- Edge-level: Each edge, namely each entry in the matrix, a_{ij}, is a separate probability distribution together with its complementer value $1 - a_{ij}$, normalized independently to 1. In this case each edge is assumed to be independent from the rest of the network. In this case both the adjacency matrix of the existing edges A, and the adjacency matrix of the non-existing edges $1 - A$ is used. In strong contrast to the network-level description, where the probability distribution extends over $N \times N$-points for N nodes, here 2-point distributions are considered of the form $\{a_{ij}, 1 - a_{ij}\}$.

While in this paper we focused on the network-level description, the node and edge level quality functions can be straightforwardly obtained by applying our case for each probability distribution separately. Thus from our network-level quality function

$$Q = D(A||B) = \sum_{ij} a_{ij} \ln \frac{a_{ij} b_{**}}{b_{ij} a_{**}} = \sum_{ij} a_{ij} \ln \frac{a_{ij}}{b_{ij}} + a_{**} \ln \frac{b_{**}}{a_{**}} \tag{1}$$

we arrive at the following node-level quality function

$$Q_N = \sum_i D(A_i||B_i) = \sum_{ij} a_{ij} \ln \frac{a_{ij} b_{i*}}{b_{ij} a_{i*}} = \sum_{ij} a_{ij} \ln \frac{a_{ij}}{b_{ij}} + \sum_i a_{i*} \ln \frac{b_{i*}}{a_{i*}} \tag{2}$$

and edge-level quality function

$$Q_E = \sum_{ij} D(A_{ij}||B_{ij}) = \sum_{ij} a_{ij} \ln \frac{a_{ij}}{b_{ij}} + \sum_{ij} (1 - a_{ij}) \ln \frac{1 - a_{ij}}{1 - b_{ij}} \ . \tag{3}$$

While for visualization the probabilistic approach appears in the literature at all the network [41], node [40] and edge [42, 49] levels, for coarse-graining we are only aware of the network [25, 26] and edge [24, 38] level descriptions. The interesting lack of node-level approaches can be better understood in our framework due to the fact, that for coarse-graining the Q_N quality function gives the same results as the Q quality function for the network-level approach due to the degree preservation in the process.

Here we note, that the network-level probabilistic interpretation usually simply assumes, that the interaction strengths are proportional to (or at least a proxy of) the chance of randomly observing an interaction between the nodes (as applied in our case for the Zachary network [52]), without assuming the independence of the nodes or edges. As for the human diseasome network [62], the edge weights have been directly constructed as co-occurrence values of two diseases over associated genes in perfect accordance to our network-level framework, without any additional assumptions.

In the following we review the most related methods in the literature in somewhat more details to give a clear picture about the similarities and differences.

B. Cross-entropy methods for visualization

Although the minimization of $D(A||B)$ appears in the *minimal discrimination information* approach – also known as the *minimum cross-entropy* (MinxEnt) approach by Kullback [53] –, there the goal is the opposite of ours, namely to find the optimal 'real' distribution, A, while the 'approximate' distribution, B, is kept fixed. In this sense, our optimization is an *inverse* MinxEnt problem [54]. Here we mention, that this kind of inverse optimization appears also as a refinement step to improve the importance sampling in Monte Carlo methods (for highly restricted A-s), under the name of *cross-entropy method* [55].

Here we note, that the concept of cross-entropy have already appeared in the field of graph drawing, such as in the methods of refs. [42, 49]. Besides differences in the final quality function, the most important difference between these methods and ours is, that in our case the relative entropy (or cross entropy) is calculated at the network-level, while these methods operate at the edge-level.

C. Stochastic Neighbor Embedding for visualization

The Stochastic Neighbor Embedding (SNE) [40] is a high-dimensional data visualization tool based on minimizing the Kullback-Leibler divergence between the input and the visual representation. In the case of the traditional SNE, it falls into the category of a node-level probabilistic approach, where the quality function is the sum of the Kullback-Leibler divergences of the rows, representing individual nodes. However, the symmetric SNE [41] works at the network-level, optimizing a single Kullback-Leibler divergence over the whole system.

However, amongst others there are two main differences between these methods and our approach. First, in our method the nodes are represented by extended distribution in the applied (low-dimensional) space, while in SNE and its variants the nodes are represented by points without spatial extensions. As an advantage, in our case the statistical weights of the nodes (the normalization of the distribution) are preserved and proportional to the degrees (a_{i*} row-sums) of the nodes. This way our method is able to adjust to the degrees of the nodes in strong contrast to the SNE-related methods, thus it is generally expected to be more appropriate for real-world networks with highly heterogeneous degree distributions.

Second, in our case the network is represented by the co-occurrence matrix of the probability distributions of the nodes, while in SNE the nodes are represented by a probabilistic matrix, which is obtained by an arbitrary transformation of the distances between the points in the low-dimensional space. Correspondingly, our method not only provides the coordinates of the nodes, but also their probability distribution, representing the uncertainty of the obtained positions. Moreover, in our case the extension of the distributions representing the uncertainty is also an adjustable parameter for each node in contrast to the SNE. As a minor difference, here we also mention, that in the SNE and related methods the diagonal elements are not considered to be parts of the system.

In the t-SNE method [41] the authors claim that it is beneficial to use a heavy-tailed transformation (such as the Student t-distribution) of the distances into probabilities in order to circumvent the observed "crowding" problem. Having namely fixed widths for the distributions it might frequently occur, that we want to put too many neighbors in the vicinity of a given node, while there is simply not enough space for it. In principle, no matter what transformation or distribution we choose for the nodes in the visualization, if the degrees are sufficiently large (as in scale-free networks), we always encounter this problem. This way, the choice of heavy-tailed distributions or transformation rules might generally somewhat reduce the problem, but will not be able to solve it. On the other hand, the crowding problem is trivially solved by adjusting also the spatial extension of the nodes, for any chosen distribution functions, as used in our method. We also note, that in contrast to our general method, the t-SNE approach cannot be applied in $d > 3$ dimensions due to the heavy tail of the Student t-distribution. Nevertheless, it is still an interesting open problem to search for (normalizable) heavy-tailed distributions in our methodology for an even more improved representation of scale-free networks compared to the simple Gaussian case considered above. As mentioned before, our approach also adjusts the statistical weight of each node according to the degree, which again helps to treat the situations with heterogeneous degrees.

However, in the simplest case of Gaussian distributions of equal variance (while only optimizing for the positions) and leaving out the diagonal entries, the formulas for our optimization and for the symmetric SNE coincide when the sum of each row (the degree os each node) is the same, thus in this special case (up to differences in the optimization heuristics) both methods yield the same results.

As an additional significant improvement, in our paper we also presented the hierarchical visualization, being the natural combination of our visualization and coarse-graining. As discussed in the text, the hierarchical approach is expected to produce layouts of much higher quality for large networks, without a significant increase in the computational time. At last, we note, that the t-SNE approach has been significantly improved recently [50] by applying the Barnes-Hut approximation [45], leading to a computational complexity of $O(N \log N)$ for N nodes, enabling the technique to study networks containing $> 10^7$ nodes. Due to the similarities with the t-SNE the same runtime and system sizes can be reached even in our case in the future enabling the analyses of massively large-scale networks.

D. Stochastic block-models for coarse-graining

Karrer and Newman [25] suggested an improved stochastic block-model (SBM) for the identification of structural patterns in graphs. In this generative model they start from the network-level probabilistic approach and write down the probability of the input matrix assuming that it comes from a given block-model. The improvement comes from the fact that the degrees of the nodes are kept fixed (on average) compared to traditional stochastic block-models, leading to much less powerful results.

In the degree-corrected SBM, when looking for partitions of the input matrix with a given number of clusters, the maximum probability (likelihood) solution coincides to the one having the minimal Kullback-Leibler divergence, $D(A||B)$, exactly as in our case. Recently it turned out [26] that for bipartite graphs it leads to higher quality results, if the bipartite structure is *a priori* enforced, instead of letting the method to learn it during the optimization.

Since our coarse-graining approach is formulated for the more general case including overlapping partitions, the state-of-the-art degree-corrected SBM can be viewed as a special case of our general coarse-graining method. As a practical difference, in our case we apply the coarse-graining hierarchically, not only at a given number of clusters. We note, however, that the hierarchical approach at a fixed number of clusters gives in general slightly different results from the direct optimization at the same number of clusters. Computationally this is not surprising, since the hierarchical approach has a polynomial run-time, while the clustering problem is known to be NP-hard. Based on this observation one might think, that the direct clustering is superior to the hierarchical approach, which is true in quality (D value), but not entirely true in purpose. The reason is, that the aim in the hierarchical coarse-graining is to find a dendrogram, or global hierarchical description, which is as optimal as possible at *all* scales of the network, not only at a fixed scale. This way the obtained dendrogram might not be optimal at all individual scales, while providing a much more detailed, global representation about the network.

Here we mention, that in the mathematical literature concentrated around graph-limits and graphons [38] and in the case of benchmark graphs for clustering [24], the term SBM has a different meaning. Namely, in these works, the SBM is formulated in the edge-level probabilistic framework, assuming the independence of all the edges from each other, in strong contrast to the network-level description.

E. Non-negative matrix factorization

While in the case of coarse-graining the aim is to fuse together parts of the input matrix, in the powerful technique of Non-negative matrix factorization [32] the aim is to divide the existing parts into subunits, which appear to be together more often. This way the goal is to find the most relevant building blocks. Given the number of blocks to use, r, the NMF uses a quality function, reminiscent to the $D(A||B)$ Kullback-Leibler divergence in our studies

$$F = -D(A||B) + a_{**} \ln b_{**} - b_{**} \ . \tag{4}$$

Here the first term is independent of b_{**} and the second term only fixes the value of b_{**} to be equal to a_{**}, thus the optimization is practically equivalent to the minimization of $D(A||B)$. As in our case A (and B) can be a non-symmetric matrix of size $N \times r$. The main difference lies in the choice of the representation B, which is chosen to be $B = WH$, where both W $(N \times r)$ and H $(r \times M)$ are to be found, having non-negative matrix elements, with a fixed number of building blocks, r. The idea is to model the input matrix, A as a linear combination (W) of appropriate hidden variables, H. Although this is a hard simultaneous optimization problem for W and H, for practical applications there is an efficient iterative approach to find locally optimal solutions, starting from random initial conditions [32].

II. NUMERICAL OPTIMIZATION FOR VISUALIZATION

For the numerical optimization of the network layout, we have implemented a simple, general purpose simulated annealing scheme. For Gaussian distributions we have also worked out a much faster Newton-Raphson update, which has been also applied in the Kamada-Kawai method. In practice, we used a separate Newton-Raphson iteration step for the d coordinates of the nodes in d spatial dimensions and for the σ_i widths and h_i normalizations of the distributions.

In each iteration step of the Newton-Raphson method, the node with the largest gradient amplitude ($||J||$) was updated in the direction and with a parameter step size, obtained by the second derivative matrix, $\mathcal{F}$ as $-\mathcal{F}^{-1}J$. Since $\mathcal{F}$ is not always positive definite, special care was needed when the relative entropy increased in such a step. In such a case, a sufficiently small step size was applied in the direction of the gradient vector, instead. This way our technique has the same computational complexity as the widely applied Kamada-Kawai method (after the initial calculation of pairwise graph-theoretic distances).

While the original, input matrix is given by A, the visualization generates the matrix of the pairwise overlaps of the node distributions, marked as B. In our approach we minimize the relative entropy between the two distributions, $D(A||B)$, which measures the extra description length, when B is used to encode the data described by A,

$$D(A||B) = \sum_{ij} a_{ij} \ln \frac{a_{ij} b_{**}}{b_{ij} a_{**}} \geq 0 \; . \tag{5}$$

Here an asterisks indicates and index for which we summed up. During optimization the a_{ij} matrix elements of the A input matrix were kept fixed, while the values of b_{ij} changed due to the variation of the x_i, y_i, σ_i (and h_i) parameters of the d-dimensional Gaussian distributions of the nodes, given by

$$\rho(\{x_i^0\}, \sigma, n) = \frac{n}{\sqrt{(2\pi)^d}} \exp\left(-\frac{\sum_{i=1}^d (x_i - x_i^0)^2}{2\sigma^2}\right) . \tag{6}$$

The overlap matrix elements of the node distributions in $d = 2$ dimensions, with notations x and y for the two coordinates, were given by

$$b_{ij} = \frac{h_i h_j}{2\pi(\sigma_i^2 + \sigma_j^2)} \exp\left(-\frac{(x_i - x_j)^2 + (y_i - y_j)^2}{2(\sigma_i^2 + \sigma_j^2)}\right) . \tag{7}$$

A. Newton-Raphson update in 2 dimensions

For a Newton-Raphson iteration step we need to calculate the first and second derivatives of the D relative entropy as the function of the parameters of each node.

1. *Updating the coordinates*

When differentiating according to the coordinates, we obtain

$$\frac{\partial b_{kj}}{\partial x_k} = -\frac{x_k - x_j}{\sigma_k^2 + \sigma_j^2} b_{kj} \; , \tag{8}$$

$$\frac{\partial D}{\partial x_k} = -2a_{**} \sum_j \frac{x_k - x_j}{\sigma_k^2 + \sigma_j^2} \left(\frac{b_{kj}}{b_{**}} - \frac{a_{kj}}{a_{**}}\right) . \tag{9}$$

From this we can see, that $\frac{b_{kj}}{b_{**}} > \frac{a_{kj}}{a_{**}}$ induces a repulsive force, while the opposite case leads to an attractive force. In order to have an efficient numerical implementation we introduce the following variables.

$$\alpha_{kj}^x = -2a_{**} \frac{x_k - x_j}{\sigma_k^2 + \sigma_j^2} b_{kj} \; , \tag{10}$$

$$\beta_{kj}^x = -2 \frac{x_k - x_j}{\sigma_k^2 + \sigma_j^2} a_{kj} \; . \tag{11}$$

Here the superscript x indicates, that we now consider the x direction in the formulas. This way the J gradient vector has the following x-component

$$j_x \equiv \frac{\partial D}{\partial x_k} = \frac{\alpha^x_{k*}}{b_{**}} - \beta^x_{k*} \ . \tag{12}$$

Consequently, while using α^x and β^x, $\frac{\partial D}{\partial x_k}$ can be calculated in $\mathcal{O}(N)$ time $\forall k$, instead of the $\mathcal{O}(N^2)$ approach of a direct evaluation. For the y direction the same formulas apply with the substitution, $x \leftrightarrow y$.

During the Newton-Raphson method that node, k, was updated, for which $||J|| \equiv j_x^2 + j_y^2$ was the largest. The $\mathcal{F}$ second derivative matrix had the following elements at a given node, k.

$$\begin{aligned} f_{xx} \equiv \frac{\partial^2 D}{\partial x_k^2} = -2\frac{a_{**}}{b_{**}}\sum_j \frac{b_{kj}}{\sigma_k^2+\sigma_j^2} + 2\sum_j \frac{a_{kj}}{\sigma_k^2+\sigma_j^2} \\ -\frac{(\alpha^x_{k*})^2}{2a_{**}b_{**}^2} - \frac{1}{b_{**}}\sum_j \frac{x_k - x_j}{\sigma_k^2+\sigma_j^2}\alpha^x_{kj} \ . \end{aligned} \tag{13}$$

$$f_{xy} \equiv \frac{\partial^2 D}{\partial x_k \partial y_k} = -2\frac{\alpha^x_{k*}\alpha^y_{k*}}{2a_{**}b_{**}^2} - \frac{1}{b_{**}}\sum_j \frac{y_k - y_j}{\sigma_k^2+\sigma_j^2}\alpha^x_{kj} \ . \tag{14}$$

In the Newton-Raphson method the step size in the x and y directions were automatically given by the vector $-\mathcal{F}^{-1}J$, if $\Delta \equiv f_{xx}f_{yy} - f_{xy}^2 \neq 0$. As a result, in the x- and y-directions we obtained

$$\delta_x = \frac{1}{\Delta}(f_{xy}j_y - f_{yy}j_x), \ \delta_y = \frac{1}{\Delta}(f_{xy}j_x - f_{xx}j_y) \ . \tag{15}$$

Since $\mathcal{F}$ is not always positive definite (not even in the traditional Kamada-Kawai method), special care was needed when the relative entropy increased in such a step. In such a case, a sufficiently small step size was applied in the direction of the gradient vector, instead of the direction given by $\mathcal{F}$. In our implementation we started with the same step size as before and iteratively kept dividing it by two, until the relative entropy decreased.

2. Updating the widths

The widths were updated separately in a similar manner (there was only one variable at each node). In order to have an efficient implementation, we first introduced the following variable

$$\gamma_{kj} = \frac{\sigma_k}{\sigma_k^2+\sigma_j^2}\left(\frac{(x_k-x_j)^2+(y_k-y_j)^2}{\sigma_k^2+\sigma_j^2} - 2\right) \ , \tag{16}$$

with which

$$\frac{\partial b_{kj}}{\partial \sigma_k} = b_{kj}\gamma_{kj} \ . \tag{17}$$

$$\frac{\partial D}{\partial \sigma_k} = -2\sum_j a_{kj}\gamma_{kj} + 2\frac{a_{**}}{b_{**}}\sum_j b_{kj}\gamma_{kj} \ . \tag{18}$$

The second derivative at a given node k was

$$\begin{aligned} \frac{\partial^2 D}{\partial \sigma_k^2} = -2\sum_j \frac{a_{kj}}{\sigma_k^2+\sigma_j^2}\epsilon_{kj} - 2\frac{a_{**}}{b_{**}}\sum_j \frac{b_{kj}}{\sigma_k^2+\sigma_j^2}\epsilon_{kj} \\ -\frac{4a_{**}}{b_{**}^2}\left(\sum_j b_{kj}\gamma_{kj}\right)^2 + \frac{2a_{**}}{b_{**}}\sum_j b_{kj}\gamma_{kj}^2 \ , \end{aligned} \tag{19}$$

where we used the notation

$$\epsilon_{kj} = \gamma_{kj}\frac{\sigma_j^2 - 2\sigma_k^2}{\sigma_k} - \frac{2\sigma_k^2}{\sigma_k^2+\sigma_j^2} \ . \tag{20}$$

3. Updating the normalizations

Although in many applications it is more natural to keep the normalizations fixed at their original value, it generally leads to improved representations if we update the h_i normalization values as well during the optimization, so we provide here the details for these steps.

$$\frac{\partial b_{kj}}{\partial h_k} = \frac{b_{kj}}{h_k} \, , \tag{21}$$

$$\frac{\partial D}{\partial h_k} = \frac{1}{b_{**}} \frac{2a_{**} b_{k*}}{h_k} - \frac{2a_{k*}}{h_k} \, . \tag{22}$$

The second derivative at a given node k was

$$\frac{\partial^2 D}{\partial h_k^2} = -\frac{4a_{**} b_{k*}^2}{h_k^2 b_{**}^2} + \frac{2a_{k*}}{h_k^2} \, . \tag{23}$$

B. The case of diagonal elements

The above formulas hold for the diagonal b_{ii} self-overlap elements as well. However, the b_{ii} values do not change during repositioning the nodes, but only by updating the σ_i widths or h_i normalizations of the Gaussians. Nevertheless, in practice, special care may be needed for the diagonal elements, describing the probability of the co-occurrence of an element with itself. If the nodes represent individual entities in A, rather than some properties or groups, then such self co-occurrences are impossible leading to $a_{ii} \equiv 0$, which can be included in the representation scheme as well, by requiring $b_{ii} \equiv 0$. While the solution of this case is rather straightforward, for the sake of simplicity we omitted its detailed study.

III. VISUALIZATION OF LARGER-SCALE EMPIRICAL NETWORKS

In this section we illustrate the applicability of our visualization approach for some empirical networks containing more than $10,000$ nodes, namely the high energy physics collaboration network [63] and the secure information sharing over a PGP network [64]. In both cases we consider the largest connected components and provide the number of nodes and edges accordingly. For simplicity, here we use the Newton-Raphson update for the positions only.

A. Collaboration network: High Energy Physics - Phenomenology

This undirected, unweighted network containing $N = 11,204$ nodes and $E = 117,649$ edges covers the collaboration between authors of manuscripts submitted to the HEP-PH (High Energy Physics - Phenomenology) section of the arXiv e-print server from January 1993 to April 2003 (124 months) [63]. Two authors are connected, if they published together a paper.

B. PGP network

This undirected, unweighted network shows the secure information interchange through the PGP (Pretty Good Privacy) algorithm of $N = 10,680$ users as nodes nodes, leading to $E = 24,316$ edges [64].

IV. ALTERNATIVE FORMULATION OF COARSE-GRAINING

In this section we show a simple, intuitive interpretation of our coarse-graining approach.

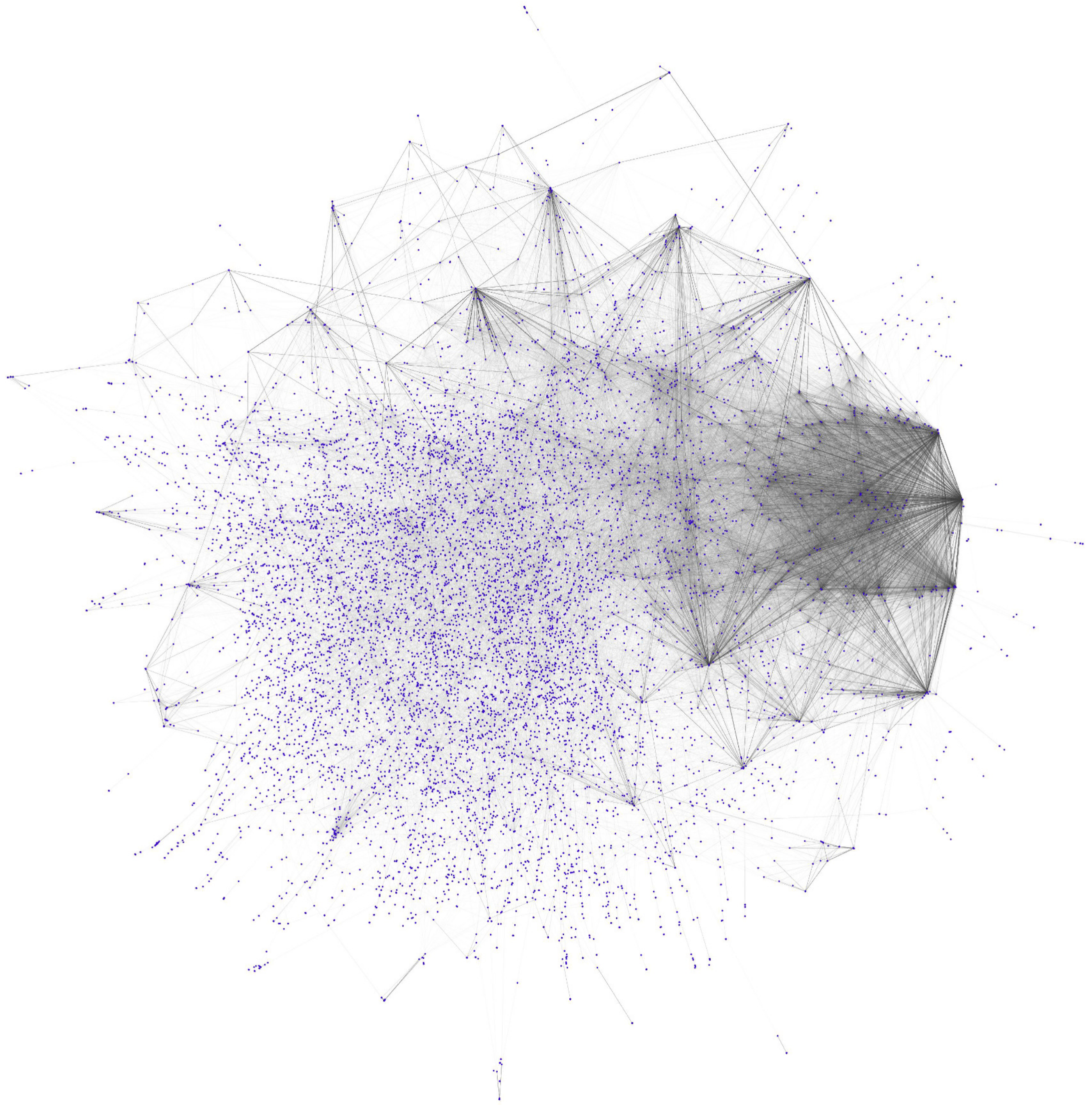

Supplementary Fig. 1: **Collaboration network.** Visualization of the collaboration in the "High Energy Physics - Phenomenology" section of the arXiv pre-print server from January 1993 to April 2003, containing $N = 11,204$ nodes and $E = 117,649$ edges.

A. Coarse-graining the rows

A grouping or coarse-graining, M, of the rows of the input matrix A can be generally described by the fusion matrix U as

$$m_{ij} = \sum_k u_{ik} a_{kj} \ , \tag{24}$$

where $u_{*k} = 1$, $\forall k$. Instead of this reduced size matrix, in our coarse-graining we used a (practically equivalent), averaged out representation, B, of the original size given by the elements

$$b_{ij} = a_{i*} \sum_k u_{ki} \frac{m_{kj}}{m_{k*}} \ . \tag{25}$$

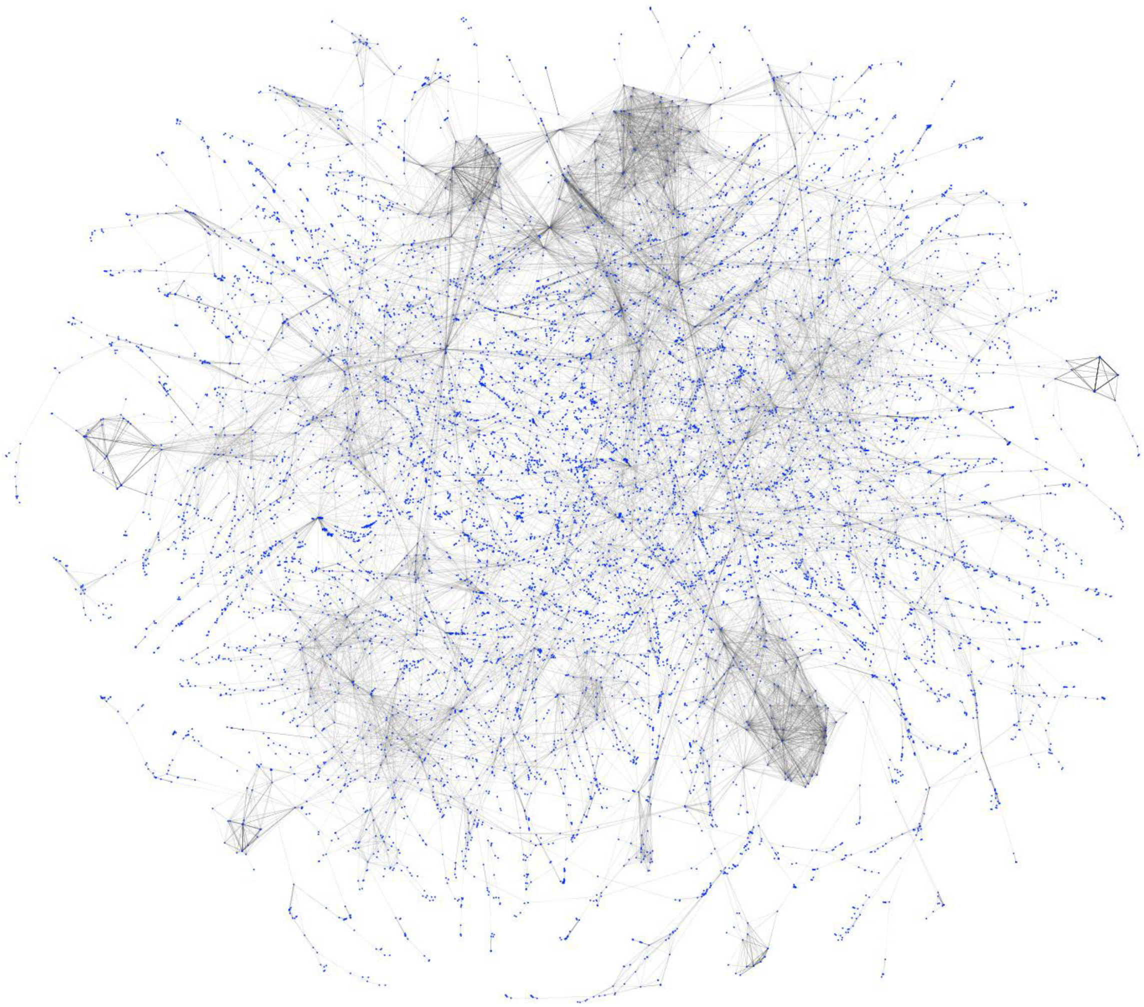

Supplementary Fig. 2: **PGP network of information sharing.** This undirected, unweighted network contains $N = 10,680$ nodes and $E = 24,316$ edges, connected in a complex, heterogeneous way, as unveiled by our visualization.

By considering partitionings of the rows, without overlaps, each row i had a unique label $\sigma(i)$ yielding its cluster. With this notation

$$b_{ij} = a_{i*} \frac{m_{\sigma(i)j}}{m_{\sigma(i)*}} . \tag{26}$$

By substituting this into Eq. (5), and changing the indices $\sigma(i) \to i$ we arrive at

$$D = \sum_{ij} a_{ij} \ln \frac{a_{ij}}{a_{i*}} - \sum_{ij} m_{ij} \ln \frac{m_{ij}}{m_{i*}} , \tag{27}$$

which is simply

$$D = I(R, C) - I(r, C) , \tag{28}$$

where r means the coarse-grained set of rows, R. Since the $I(R, C) \equiv D_0$ mutual information can be interpreted as the amount of structural 'signal' in the original data, D is the amount of lost structural signal during coarse-graining.

B. Coarse-graining both the rows and columns

The simultaneous coarse-graining of the rows and columns of A was given by the matrix elements

$$w_{ij} = \sum_k u_{ik} v_{jl} a_{kl} \ , \tag{29}$$

where $v_{*l} = 1$, $\forall l$. The averaged out representation, B, of the original size was given in this case by the elements

$$b_{ij} = a_{i*} a_{*j} \sum_{kl} u_{ki} v_{lj} \frac{w_{kl}}{w_{k*} w_{*l}} \ . \tag{30}$$

By considering partitionings, this can be written in the form of

$$b_{ij} = a_{i*} a_{*j} \frac{w_{\sigma(k)\sigma(l)}}{w_{\sigma(k)*} w_{*\sigma(l)}} \ . \tag{31}$$

By substituting this into Eq. (5), and changing the indices as before, we arrive at

$$D = \sum_{ij} a_{ij} \ln \frac{a_{ij}}{a_{i*} a_{*j}} - \sum_{ij} w_{ij} \ln \frac{w_{ij}}{w_{i*} w_{*j}} \ , \tag{32}$$

which is simply

$$D = I(R,C) - I(r,c) \ , \tag{33}$$

where r (c) means the coarse-grained R (C). Thus, it is true also in this case, that D can be interpreted as the amount of lost structural signal during coarse-graining. For a graphical representation of these considerations see Fig. 1. of the Supplementary Information.

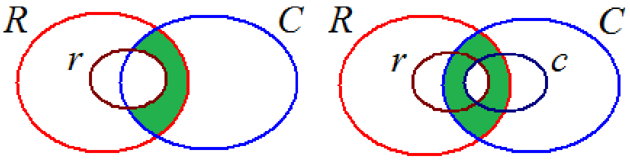

Supplementary Fig. 3: **Graphical representation of the relative entropy, D, used in the hierarchical coarse-graining.** In the information content diagram the shaded (green) area indicates D, which is found to be the amount of the lost mutual information between the rows (R) and the columns (C). The coarse-grained rows and columns are denoted by r and c, respectively. Left: coarse-graining for the rows (R) only. Right: simultaneous coarse-graining of the rows and columns.

V. GREEDY OPTIMIZATION FOR COARSE-GRAINING

Since in a coarse-graining step the B representation matrix is modified, for the remaining steps the D difference should be updated if at least one member of the pair is neighbor of the fused elements. Although it seems to be tedious in a later step to measure D always from the original input matrix for a given (k,l) pair, there is a simple way to calculate this from the actually existing coarse-grained data alone. If D_k and D_l are the values when the rows (and columns) k and l were formed via fusion (being zero initially), then from the apparent D' value – measuring the formation of a bond directly from the coarse-grained rows k and l – we got

$$D = D_k + D_l + D' \ . \tag{34}$$

This results is valid both for the coarse-graining of the rows and for the simultaneous coarse-graining of both the rows and columns.

A. Coarse-graining of the rows

In the following we summarize the numerical details of coarse-graining the rows of a matrix with N_r rows and N_c columns. For each pair of rows the δ difference of the D relative entropy value for the fusion step could be calculated independently from the other pairs. Thus after a fusion step only the δ values of the new row with the rest of the rows were needed to be calculated in $\mathcal{O}(N_c)$ time. Since in each step the pair with the lowest δ value was fused, we needed to select the lowest value before each step, which could be conveniently done with a binary heap data structure in $\mathcal{O}(\ln N_r)$ time. Altogether we finished in $\mathcal{O}\left(N_r^2 N_c\right)$ time.

B. Coarse-graining of both the rows and columns

In the following we overview the numerical details of the simultaneous coarse-graining of both the rows and columns of a symmetric matrix with N rows and columns. In this case the fusion of two node pairs is generally not independent, thus besides calculating the δ values of the new row, all the other values may be needed to be updated. Fortunately, this can be done in constant time between rows i and j. After the fusion of rows a and b, δ_{ij} must be increased by $2\Delta_{ij}$, where

$$\begin{aligned}\Delta_{ij} &= -w_{ia}\ln w_{ia} - w_{ja}\ln w_{ja} - w_{ib}\ln w_{ib} - w_{jb}\ln w_{jb}\\ &+(w_{ia}+w_{ja})\ln(w_{ia}+w_{ja}) + (w_{ib}+w_{jb})\ln(w_{ib}+w_{jb})\\ &+(w_{ia}+w_{ib})\ln(w_{ia}+w_{ib}) + (w_{ja}+w_{jb})\ln(w_{ja}+w_{jb})\\ &-(w_{ia}+w_{ja}+w_{ib}+w_{jb})\ln(w_{ia}+w_{ja}+w_{ib}+w_{jb})\ .\end{aligned} \tag{35}$$

Altogether the whole process took $\mathcal{O}(N^3)$ time.

C. Basic notations for coarse-graining

With the notations $m_{ij} = \sum_k u_{ik}a_{kj}$, $n_{ij} = \sum_k a_{ik}v_{jk}$ and $w_{ij} = \sum_{kl} u_{ik}a_{kl}v_{jl}$ the relevant entropy measures can be expressed as follows.

$$S(R) = -\sum_i a_{i*}\ln\frac{a_{i*}}{a_{**}},\ S(C) = -\sum_i a_{*i}\ln\frac{a_{*i}}{a_{**}} \tag{36}$$

$$S(r) = -\sum_i m_{i*}\ln\frac{m_{i*}}{a_{**}}\,;S(c) = -\sum_i n_{*i}\ln\frac{n_{*i}}{a_{**}} \tag{37}$$

$$S(r,C) = -\sum_{ij} m_{ij}\ln\frac{m_{ij}}{a_{**}},\ S(R,c) = -\sum_{ij} n_{ij}\ln\frac{n_{ij}}{a_{**}} \tag{38}$$

$$S(R,C) = -\sum_{ij} a_{ij}\ln\frac{a_{ij}}{a_{**}},\ S(r,c) = -\sum_{ij} w_{ij}\ln\frac{w_{ij}}{a_{**}} \tag{39}$$

From these we could deduce the used measures of mutual information for any X and Y as $I(X,Y) = S(X) + S(Y) - S(X,Y)$.

[1] Newman, M. E. J. Networks: An Introduction. (Oxford Univ. Press, 2010).

[2] Albert, R. & Barabási, A.-L. Statistical mechanics of complex networks. *Reviews of Modern Physics* **74,** 47-97 (2002).

[3] Newman, M. E. J. Assortative mixing in networks. *Phys. Rev. Lett.* **89,** 208701 (2002).

[4] Reshef, D. N. et al. Detecting novel associations in large data sets. *Science* **334,** 1518-1524 (2011).

[5] Girvan, M. & Newman, M. E. J. Community structure in social and biological networks. *Proc. Natl Acad. Sci. USA* **99,** 7821-7826 (2002).

[6] Newman, M. E. J. Communities, modules and large-scale structure in networks. *Nature Physics* **8,** 25-31 (2012).

[7] Fortunato, S. Community detection in graphs. *Phys. Rep.* **486,** 75-174 (2010).

[8] Kovács, I. A., Palotai, R., Szalay, M. S. & Csermely, P. Community landscapes: an integrative approach to determine overlapping network module hierarchy, identify key nodes and predict network dynamics. *PLoS ONE* **5,** e12528 (2010).

[9] Olhede, S. C. & Wolfe, P. J. Network histograms and universality of blockmodel approximation. *Proc. Natl Acad. Sci. USA* **111,** 14722-14727 (2014).

[10] Bickel P. J., Chen A. A nonparametric view of network models and Newman-Girvan and other modularities. *Proc. Natl. Acad. Sci. USA* **106** (50):2106821073. (2009).

[11] Bickel P. J., Sarkar P. Hypothesis testing for automated community detection in networks. arXiv:1311.2694. (2013) (Date of access:15/02/2015).

[12] King, I. P. An automatic reordering scheme for simultaneous equations derived from network analysis. *Int. J. Numer. Methods*, **2,** 523-533 (1970).

[13] George A. & Liu, J. W.-H. Computer solution of large sparse positive definite systems. (Prentice-Hall Inc, 1981).

[14] West, D. B. Introduction to graph theory 2nd edn. (Prentice-Hall Inc, 2001).

[15] Song, C., Havlin, S. & Makse, H. A. Self-similarity of complex networks. *Nature* **433,** 392-395 (2005).

[16] Gfeller, D. & De Los Rios, P. Spectral coarse graining of complex networks. *Phys. Rev. Lett.* **99,** 038701 (2007).

[17] Sales-Pardo, M., Guimera, R., Moreira, A. A. & Amaral L. A. N. Extracting the hierarchical organization of complex systems. *Proc. Natl. Acad. Sci. USA* **104,** 15224-15229 (2007).

[18] Ravasz, E., Somera, A. L., Mongru, D. A., Oltvai, Z. N. & Barabási, A.-L. Hierarchical organization of modularity in metabolic networks. *Science* **297,** 1551-1555 (2002).

[19] Radicchi, F., Ramasco, J. J., Barrat, A. & Fortunato, S. Complex networks renormalization: flows and fixed points. *Phys. Rev. Lett.* **101,** 148701 (2008).

[20] Rozenfeld, H. D., Song, C. & A. Makse, H. A. Small-world to fractal transition in complex networks: a renormalization group approach. *Phys. Rev. Lett.* **104,** 025701 (2010).

[21] Walshaw, C. A multilevel approach to the travelling salesman problem. *Oper. Res.*, **50,** 862-877 (2002).

[22] Walshaw, C. Multilevel refinement for combinatorial optimisation problems. *Annals of Operations Research* **131,** 325-372 (2004).

[23] Ahn, Y.-Y., Bagrow J. P. & Lehmann S. Link communities reveal multiscale complexity in networks *Nature* **1038**, 1-5 (2010).

[24] Lancichinetti, A., Fortunate, S. & Radicchi, F., Benchmark graphs for testing community detection algorithms, *Phys. Rev. E* **78,** 046110 (2008).

[25] Karrer, B. & Newman, M. E. J., Stochastic blockmodels and community structure in networks. *Phys. Rev. E* **83,** 016107 (2011).

[26] Larremore, D. B., Clauset, A. & Jacobs, A. Z., Efficiently inferring community structure in bipartite networks. *Phys. Rev. E* **90,** 012805 (2014).

[27] Di Battista, G., Eades, P., Tamassia, R. & Tollis, I.G. Graph Drawing: Algorithms for the Visualization of Graphs. (Prentice-Hall Inc, 1998).

[28] Kobourov, S. G. Spring embedders and force-directed graph drawing algorithms. arXiv:1201.3011 (2012) (Date of access:15/02/2015).

[29] Graph Drawing, Symposium on Graph Drawing GD'96 (ed North, S.), (Springer-Verlag, Berlin, 1997).

[30] Garey, M. R. & Johnson, D. S. Computers and Intractability: A Guide to the Theory of NP-Completeness. (W.H. Freeman and Co., 1979).

[31] Kinney, J. B. & Atwal, G. S. Equitability, mutual information, and the maximal information coefficient. *Proc. Natl. Acad. Sci. USA* **111,** 3354-3359 (2014).

[32] Lee, D. D., &Seung, H. S., Learning the parts of objects by non-negative matrix factorization. *Nature* **401,** 788-791 (1999).

[33] Slonim, N., Atwal, G. S., Tkačik, G. & Bialek, W. Information-based clustering. *Proc. Natl. Acad. Sci. USA* **102,** 18297-18302 (2005).

[34] Rosvall, M. & Bergstrom, C. T. An information-theoretic framework for resolving community structure in complex networks. *Proc. Natl. Acad. Sci. USA* **104,** 7327-7331 (2007).

[35] Rosvall, M., Axelsson, D. & Bergstrom, C. T. The map equation. *Eur. Phys. J. Special Topics* **178,** 13 -23 (2009).

[36] Zanin, M., Sousa, P. A. & Menasalvas, E. Information content: assessing meso-scale structures in complex networks. *Europhys. Lett.* **106,** 30001 (2014).

[37] Allen, B., Stacey, B. C. & Bar-Yam, Y. An information-theoretic formalism for multiscale structure in complex systems. arXiv:1409.4708 (2014) (Date of access:15/02/2015).

[38] Lovász, L., Large networks and graph limits, volume 60 of American Mathematical Society Colloquium Publications. American Mathematical Society, Providence, RI, (2012).

[39] Kullback, S. & Leibler, R. A. On information and sufficiency. *Annals of Mathematical Statistics* **22,** 79-86 (1951).

[40] Hinton, G., & Roweis, S., Stochastic Neighbor Embedding, in Advances in Neural Information Processing Systems, Vol. 15, 833-840 (The MIT Press, Cambridge, 2002).

[41] van der Maaten, L., & Hinton, G., Visualizing Data using t-SNE, *Journal of Machine Learning Research*, **9,** 2579-2605 (2008).

[42] Yamada, T., Saito, K. & Ueda, N. Cross-entropy directed embedding of network data, *Proceedings of the 20th International Conference on Machine Learning (ICML2003)*, 832-839 (2003).

[43] Grünwald, P. D., The Minimum Description Length Principle, (MIT Press, 2007).

[44] See, e.g., Cover, Th. M. & Thomas, J. A. Elements of Information Theory 1st edn, Lemma 12.6.1, 300-301 (John Wiley & Sons, 1991).

[45] Barnes, J. & Hut, P. A hierarchical O(NlogN) force-calculation algorithm. *Nature*, **324,** 446-449 (1986).

[46] Gansner, E. R., Koren, Y. & North, S. in Graph drawing by stress majorization, Vol. 3383 (ed Pach J.), 239-250 (Springer-Verlag, 2004).

[47] Fruchterman, T. M. & Reingold, E. M. Graph Drawing by Force-Directed Placement, *Software: Practice & Experience* **21,** 1129-1164 (1991).

[48] Kamada, T. & Kawai, S. An algorithm for drawing general undirected graphs. *Information Processing Letters* (Elsevier) **31,** 7-15 (1989).

[49] Estévez, P. A., Figueroa, C. J. & Saito, K. Cross-entropy embedding of high-dimensional data using the neural gas model. *Neural Networks*, **18,** 727-737 (2005).

[50] van der Maaten, L. J. P., Accelerating t-SNE using Tree-Based Algorithms. *Journal of Machine Learning Research* **15** 3221-3245 (2014).

[51] Hopcroft, J. & Tarjan, R. E. Efficient planarity testing. *Journal of the Association for Computing Machinery* **21,** 549-568 (1974).

[52] Zachary, W. W. An information flow model for conflict and fission in small groups. *Journal of Anthropological Research* **33,** 452-473 (1977).

[53] Kullback, S. Information Theory and Statistics, (John Wiley: New York, NY, USA, 1959).

[54] Kapur, J. N. & Kesavan, H. K., The inverse MaxEnt and MinxEnt principles and their applications, in Maximum Entropy and Bayesian Methods, Fundamental Theories in Physics, Springer Netherlands, **39,** 433-450 (1990).

[55] Rubinstein, R. Y., The cross-entropy method for combinatorial and continuous optimization. *Method. Comput. Appl. Probab.* **1,** 127-190 (1999).

[56] Gajer, P., Goodrich, M. T. & Kobourov, S. G. A multi-dimensional approach to force-directed layouts of large graphs, *Computational Geometry: Theory and Applications* **29,** 3-18 (2004).

[57] Harel, D. & Koren, Y. A fast multi-scale method for drawing large graphs. *J. Graph Algorithms and Applications*, **6,** 179-202 (2002).

[58] Walshaw, C. A multilevel algorithm for force-directed graph drawing. *J. Graph Algorithms Appl.*, **7,** 253-285 (2003).

[59] Hu, Y. F. Efficient and high quality force-directed graph drawing. *The Mathematica Journal*, **10,** 37-71 (2006).

[60] Szalay-Bekő, M., Palotai, R., Szappanos, B., Kovács, I. A., Papp, B. & Csermely P., ModuLand plug-in for Cytoscape: determination of hierarchical layers of overlapping network modules and community centrality. *Bioinformatics* **28,** 2202-2204 (2012).

[61] Six, J. M., & Tollis, I. G. in Software Visualization, Vol. 734, (ed Zhang, K.) Ch. 14, 413-437 (Springer US, 2003).

[62] Goh, K.-I. et al. The human disease network. *Proc. Natl. Acad. Sci. USA* **104,** 8685-8690 (2007).
Goh, K.-I., Cusick, M., Valle, D., Childs, B., Vidal, M. & Barabási, A.-L., The human disease network (the human diseasome)., (2006) (Date of access:15/02/2015)
`http://www.barabasilab.com/pubs/CCNR-ALB_Publications/200705-14_PNAS-HumanDisease/Suppl/index.htm`

[63] Leskovec, J., Kleinberg, J. & Faloutsos, C., Graph Evolution: Densification and Shrinking Diameters. ACM Transactions on Knowledge Discovery from Data (ACM TKDD), 1(1), (2007). Data is available at: `http://snap.stanford.edu/data/ca-HepPh.html`

[64] Boguña, M., Pastor-Satorras, R., Diaz-Guilera, A., & Arenas, A., Models of social networks based on social distance attachment. *Phys. Rev. E*, **70,** 056122 (2004). Data is available at: `http://deim.urv.cat/ alexandre.arenas/data/welcome.htm`